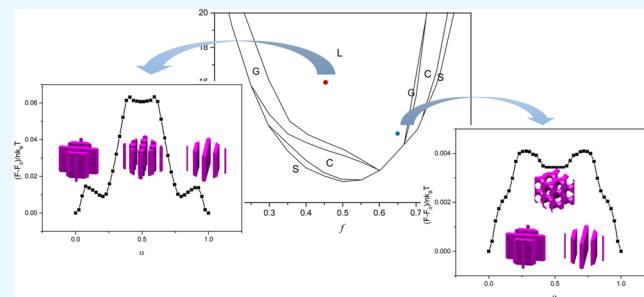


Target-Directed Design of Phase Transition Path for Complex Structures of Rod–Coil Block Copolymers

Jingyu Shao, Nuofei Jiang, Hongdong Zhang, Yuliang Yang, and Ping Tang*^{ID}

State Key Laboratory of Molecular Engineering of Polymers, Department of Macromolecular Science, Fudan University, Shanghai 200433, China

ABSTRACT: We apply the string method to the self-consistent mean-field theory framework of the rod–coil block copolymer system to calculate the minimum energy pathways in the rearrangement transitions of lamellae and cylinders with different orientations under certain epitaxial growth relationship. Metastable phases appearing in the reordering transition pathway tend to form the structure at low χN side of the order–order transition boundary compared with the initial phase. In particular, for complex network, metastable phases, such as single gyroid and perforated lamellae, need to select a rearrangement transition between lamellae or cylinders near the order–disorder transition boundary with the same epitaxial growth relationship but different orientations. It is confirmed that this strategy for obtaining complex metastable phases by rational design of rearrangement transition between specific phases in the phase diagram can be applied to a wide range of χN as well as the coil–coil block copolymer system. We further investigate the rearrangement transition behavior combining with the analysis of contribution from the free energy, entropy, degree of mixing between different blocks, and the average orientation degree of rods during the phase transitions. Based on this mechanism, we have developed a target-directed design strategy for constructing self-assembled metastable structures of rod–coil block copolymers.



INTRODUCTION

Block copolymer melt and solution systems have been studied as classic self-assembled materials for many years due to their simple preparation methods, good mechanical properties, and abundant periodic ordered microphase separated structures.^{1–5} Various means cause the self-assembly behavior of block copolymer systems to be more complicated and diverse, such as increasing the number of different chemical blocks,^{6,7} changing the rigidity of blocks,⁸ regulating the block sequence distribution and chain topologies (linear, star,^{9,10} comb,¹² and ring chains¹⁰), and blending with different types of polymers¹³ and nanoparticles.¹⁴ Among them, the block copolymer that contains a certain chain rigidity has great applications in many fields, including light-emitting diodes (LEDs),¹⁵ polymer solar cells,¹⁶ and high-modulus polymer.¹⁷ Research studies on the block copolymer with rigid chains have attracted more and more attention, which is formed by covalently linking two different rigidity blocks, such as semiconductor polymers with the conjugate structure of $\pi-\pi$,^{18–20} block copolymers containing aromatic groups,^{21,22} liquid crystal polymers,^{23–25} and various biological macromolecules.^{26–29} In contrast to coil–coil block copolymers, the block copolymer with rigid chains has a large geometrical asymmetry effect between different rigidity blocks and the strong anisotropic orientation interaction between rigid segments, as shown in Figure 1. As a result, the theoretical studies on the block copolymer containing rigid blocks are still undeveloped due to its complicated structures and wider parameter space.^{30–33} There are more and more work on the

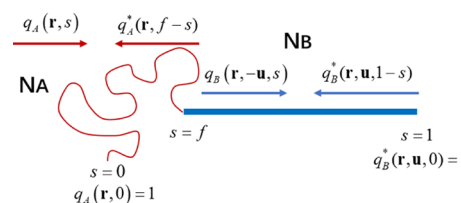


Figure 1. Rod–coil diblock copolymer model for SCFT calculations. $q_A(\mathbf{r}, s)$ and $q_B(\mathbf{r}, -\mathbf{u}, s)$ are the probability distribution function of flexible segments and rigid segments, respectively. Similarly, $q_A^*(\mathbf{r}, f-s)$ and $q_B^*(\mathbf{r}, \mathbf{u}, 1-s)$ represent the flexible segments and rigid segments probability distribution function from the other side of the copolymer chain.

self-assembly of block copolymers with rigid segments experimentally. For example, it is found that the complex phenomenon of multistage self-assembly occurs under the existence of external field.³⁴ Recent experiments show that introducing a side methyl group and a methyl group at junctions between rods and the coil blocks can prepare cylinder phases and perforated lamellar phases in solution and bulk.³⁵ The coil–rod–coil triblock terpolymer can self-assemble into complex network structures such as double diamond, single gyroid, and double primitive in solution systems.³⁶ Wiesner et al. used the

Received: September 13, 2019

Accepted: October 24, 2019

Published: November 18, 2019



coil–rod–coil block polymer with a unique self-assembly character and good physical properties to prepare the gyroid framework, which has excellent optical and electrical properties.^{37,38}

The self-consistent mean-field theory (SCFT), first proposed by Edwards,³⁹ is one of the most accurate theories on the mesoscopic scale to investigate the thermodynamic equilibrium state behaviors. The main idea of this approach is to simplify the multibody complex interaction in the practical polymer system into a situation where a single polymer chain is in the average field generated by others. The SCFT has been successfully employed to investigate the equilibrium phase behavior for the self-assembly of block copolymers with various chain architectures in bulk and under confinement.⁴⁰ Most theoretical works to date have been concentrated on the thermodynamic equilibrium self-assembly of block copolymers. However, the self-assembly behavior in practical applications is very complicated. The properties required for these materials inevitably involve nonequilibrium states, which are often a critical factor in determining the ultimate performance of the material. First, the block copolymer itself has high molecular weight, high polydispersity and thus long relaxation time, wide relaxation time spectrum, and high viscosity. It is difficult to reach the thermodynamic equilibrium state in experimental timescale, but the system is always trapped in some metastable phases. For example, the perforated lamellae (PL) have often been found in the transition pathway between different phases in experiments and have long-term stability.^{41–43} Furthermore, the processing conditions of practical polymer systems are very complicated. The presence of external field such as the magnetic field,⁴⁴ pressure field,⁴⁵ and shear field⁴⁶ during processing usually causes phase morphology changes, including the orientation of rods and the order–order transition (OOT), leading to more complex metastable phases. Recently, experiments by Kim et al. showed that different thermodynamic processing conditions will induce the appearance of complex metastable structures.⁴⁷ The phase transition also occurs under large amplitude oscillatory shearing in the block copolymer system.⁴⁸ Finally, in evolution, the molecular topologies considered by theoretical calculations are more and more complex, and thus, the equilibrium or metastable self-assembled phases are also more and more abundant.⁴⁹ In particular, the difference in free energy between different metastable structures is quite small in most cases, and weak fluctuations may induce phase transitions. Therefore, these complex metastable phases are often observed experimentally. For rod–coil block copolymers, the phase transition kinetics is even more complicated due to the effect of the geometrical asymmetry and the orientation interaction, which is a huge challenge for both experimental and theoretical work.⁵⁰

It is obvious that abundant and complex phase structures occur in the phase transition path and thus focusing on the dynamic information of the self-assembly process of block copolymers is more important, rather than the thermodynamic equilibrium state. In other words, some metastable structures in the self-assembly path have long-term stability and thus have easily been observed in experiments. The string method is exactly a powerful tool for investigating the kinetic information of phase transitions, such as minimum energy pathway (MEP). Our previous work has obtained the phase transition pathway of single networks for rod–coil block copolymers via matching the epitaxial growth relationship and employing SCFT combining with the string method.⁵¹ However, this work shows that only

under the condition of exact epitaxial growth and certain parameters, such as the reordering transition pathway between {110} lamellae with $\chi N = 13$, $\mu N = 13$, and $\beta = 2$, the target single network will appear as a long-term stability metastable phase in the rearrangement transition pathway. Obviously, it is still difficult to construct the target structure via designing kinetic pathways. In this work, based on the SCFT calculations for the phase diagram of 3D self-assembly structure, we focus on the rod–coil copolymer rearrangement transition mechanism and guide the target-directed design by searching for the kinetic pathway between specific phases. We calculate the $\chi N - f$ phase diagram for the rod–coil block copolymer with $\beta = 2$ and $\mu N = 10$ and confirm the target rearrangement transition pathway by combining the epitaxial relationship and phase diagram. Based on this method, we achieve constructing single gyroid (SG) and tetragonally packed cylinders from reordering transition between {110} lamellae and PL and body-centered cubic spheres from reordering transition between <111> cylinders in the rod–coil block copolymers. We systematically study the contribution from the entropy, contacting degree, and orientation during the reordering transitions and find that rod–coil block copolymers have a natural advantage in constructing complex network structures. In particular, the application scope of the target design strategy is further presented.

THEORY AND COMPUTATION METHODS

SCFT for Rod–Coil Block Copolymers. The SCFT based on the rod–coil chain model is the most suitable theoretical model for studying the thermodynamic equilibrium behavior on the mesoscopic scale. Here, we merely briefly show the SCFT of rod–coil blocks. Consider an incompressible rod–coil diblock copolymer system consisting of n identical copolymer chains with a volume of V . Each coil block contains N_A segments of statistical segment length a , and each rod block has N_B segments of statistical segment length b , where $b = l_R/N_B$ with l_R of each rod block length. For simplicity, assuming that rigid and flexible segments have the same bulk number density ρ_0 ($\rho_0 = nN/V$), where $N \equiv N_A + N_B$, denoting each block copolymer chain length. Obviously, the volume fraction of each coil block is $f = N_A/N$, and the rod block is $1 - f$. In the SCFT, the variable s (in unit length of N) parameterizes the chain length of diblock copolymers, where $s = 0$ indicates the beginning of the Gaussian chain, $s = f$ indicates the junction point of the two blocks, and $s = 1$ is the end of the rod block. Also, we introduce a parameter β to define a geometrical asymmetry between rigid and flexible blocks,⁵² $\beta = bN/a\sqrt{(N/6)}$, indicating the shape of rods (length-to-diameter ratio). The rods are slender when the β is large, and on the contrary, the small β corresponds to stubby rods.

As the detail of SCFT method of rod–coil copolymer was first proposed by Pryamitsyn and Ganeshan⁵³ and has been described in our previous study,⁵² we ignore the SCFT equations for rod–coil blocks and only show the system's single-chain free energy

$$\frac{F}{nk_B T} = \frac{1}{V} \int d\mathbf{r} [\chi N \phi_A(\mathbf{r}) \phi_B(\mathbf{r}) - \omega_A(\mathbf{r}) \phi_A(\mathbf{r}) - \omega_B(\mathbf{r}) \phi_B(\mathbf{r}) - \eta(\mathbf{r}) [1 - \phi_A(\mathbf{r}) - \phi_B(\mathbf{r})] - \frac{\mu N}{2} \mathbf{T}(\mathbf{r}) : \mathbf{T}(\mathbf{r}) + \mathbf{M}(\mathbf{r}) : \mathbf{T}(\mathbf{r})] - \ln Q \quad (1)$$

where $\phi_A(\mathbf{r})$ and $\phi_B(\mathbf{r})$ represent the normalized segmental density of coil and rod segments, respectively; $\omega_A(\mathbf{r})$ and $\omega_B(\mathbf{r})$ are the potential field conjugated to the density of coil and rod segments, respectively; χ is the Flory–Huggins interaction parameter; $\mathbf{M}(\mathbf{r})$ is the orientation field conjugated to the average orientation order parameter $T(\mathbf{r})$; the Maier–Saupe parameter μ indicates the orientation interaction between rods; $\eta(\mathbf{r})$ is used to guarantee the incompressibility condition of the system.

The single-chain free energy of the system can be divided into three parts: the interfacial energy $\frac{F_{\text{inter}}}{nk_B T}$, entropy $-\frac{S}{nk_B}$, and orientation interaction energy $-\frac{F_{\text{orien}}}{nk_B T}$.

$$-\frac{S}{nk_B} = \frac{1}{V} \int d\mathbf{r} \{ -\omega_A(\mathbf{r})\phi_A(\mathbf{r}) - \omega_B(\mathbf{r})\phi_B(\mathbf{r}) \\ - \eta(\mathbf{r})[1 - \phi_A(\mathbf{r}) - \phi_B(\mathbf{r})] + \mathbf{M}(\mathbf{r}) \cdot \mathbf{T}(\mathbf{r}) \} - \ln Q \quad (2)$$

$$\frac{F_{\text{inter}}}{nk_B T} = \frac{1}{V} \int d\mathbf{r} \chi N \phi_A(\mathbf{r}) \phi_B(\mathbf{r}) \quad (3)$$

$$-\frac{F_{\text{orien}}}{nk_B T} = -\frac{1}{V} \int d\mathbf{r} \frac{\mu N}{2} \mathbf{T}(\mathbf{r}) \cdot \mathbf{T}(\mathbf{r}) \quad (4)$$

where the orientation interaction energy $-F_{\text{orien}}$ is based on the Maier–Saupe interaction, with the μ value reflecting the degree of orientation between rods. When the orientation interaction energy is relatively large, the rigid blocks arrangement tends to be chaotic. The single chain partition function Q satisfies

$$Q = \frac{1}{V \int d\mathbf{u}} \int d\mathbf{r} \int d\mathbf{u} \exp \left[- \int_0^{1-f} ds \Gamma(\mathbf{r} + \beta s\mathbf{u}, \mathbf{u}) \right] q_A(\mathbf{r}, f) \quad (5)$$

where propagator $q_A(\mathbf{r}, s)$ corresponds to the flexible segments probability distribution function, which indicates the probability of finding a coil segment of s that starts from the coil end (where $s = 0$) anywhere in the system and ends at position \mathbf{r} ($0 \leq s < f$). It satisfies a modified diffusion equation of the Gaussian chain, and the initial value is $q_A(\mathbf{r}, 0) = 1$, as shown in Figure 1. Similarly, $q_A^*(\mathbf{r}, f-s)$ represents the probability of finding the coil segment s that starts from the rod–coil junction ($s = f$) and ends at position \mathbf{r} ($0 \leq s < f$). We solve the modified diffusion equation according to the Gaussian chain with the pseudospectral method⁵⁴ and use the fast Fourier transform to calculate the density and the orientation order parameters of rigid segments.

To numerically solve SCFT equations of the rod–coil system stably and accurately, we use the icosahedron triangular mesh method to deal with the orientation discretization of rods.⁵⁵ This method disperses the orientation angle on the surface of the unit sphere uniformly and does integrals on the sphere, which can improve the numerical stability for solving SCFT equations. We use the semi-implicit relaxation scheme proposed by Man et al.⁵⁶ for field iteration, which speeds up the convergence of the field and improves the numerical stability during the operational process. Semi-implicit relaxation scheme, also known as semi-implicit seidel (SIS), is proven to be more efficient and stable in studying the phase behavior of two polymer blends comparing to conventional explicit iterative methods.^{57,58} For the calculation of the rod–block concentration and orientation order parameter, we utilize the translation properties of the Fourier transform and adopt parallel computing in the Fourier space.⁵⁹

String Method. The string method, first proposed by E, Ren, and Vanden-Eijnden,^{60–62} is conveniently used to study the phase transition between metastable or stable phases for block copolymers. It is independent of our preunderstanding of the system dynamics and can obtain some kinetic information such as MEP based on the study of the free energy landscape.^{51,63–65} The metastable phases appearing in the reordering transition located in the valley of the free energy landscape and the maximum value of the MEP corresponds to the free energy barrier of transition. The valley of the free energy landscape can occupy a large range, which make the metastable phases easy to be obtained. Here, we embed the SCFT into the string method to explore the phase transition process between two different structures (including morphology and free energy) obtained by the SCFT (set as M and N), with free energy of F_0 and F_1 , corresponding to two ends of the string. The MEP is a string τ in the free energy landscape connecting two initial phases M and N . It can constraint the free energy of systems to decrease only along a direction perpendicular to the string. Besides, we apply an equal arc length during the iterative process to ensure that the order parameters of the density between adjacent phases on the string have the same difference, preventing metastable phases on the string from converging to the local minimum value during the iterative process. We use cubic spline interpolation to achieve this limit in this study, and specific implementation processes are described by E et al.⁶⁶ The distance between all adjacent order parameters $\phi_i(\mathbf{r})$ and $\phi_{i-1}(\mathbf{r})$ is defined here as $d_{i-1, i}$ ($i = 1, 2, \dots, n$)

$$d_{i-1, i} = \sqrt{\int d\mathbf{r} [\phi_i(\mathbf{r}) - \phi_{i-1}(\mathbf{r})]^2 / \int d\mathbf{r}} \quad (6)$$

where i is the discrete point of the string. For the rod–coil copolymer system, we need at least two order parameters to determine a state of the system: the chemical potential field $\omega_A(\mathbf{r})$ or $\omega_B(\mathbf{r})$ and the orientation field $\mathbf{M}(\mathbf{r})$ for rigid blocks or their density order parameter and the orientation order parameter that are conjugated to the field. Therefore, the equal arc length limit above should be applied to the two order parameters. It is worth noting that $\phi_A(\mathbf{r})$, $\phi_B(\mathbf{r})$, $\eta(\mathbf{r})$, and $\mathbf{M}(\mathbf{r})$ are not fully coupled before the self-consistent mean-field iteration reaches the equilibrium state, indicating that they can change independently of each other. In fact, we do not need to impose the equal arc length limit on too many order parameters for the numerical calculation stability. In this study, the equal arc length limit of two order parameters such as $\phi_A(\mathbf{r})$ and $\mathbf{M}(\mathbf{r})$ has found a balance between the accuracy and computational costs during the string iteration process, and the final MEP will not change with excessive equal arc length limit of other order parameters.

By calculation of the SCFT, the order parameters of two ends of the string ϕ_M and ϕ_N are known, and we can initialize the order parameters of each discrete point along the string by combining the order parameters in different ways according to different requirements. In this study, we mainly focus on metastable phases along the possible transition pathways in which the order parameters of each state along the string change simultaneously in the whole calculation cell. So, the initial fields of each state on the string are set to evolve gradually in the whole box from M to N

$$\phi_i(\mathbf{r}) = \phi_M(\mathbf{r}) + in(\phi_N(\mathbf{r}) - \phi_M(\mathbf{r})), i = 0, 1, \dots, n \quad (7)$$

where n is the number of discrete points of the string, with $n = 40$ in this work to ensure the computational efficiency and stability. After each structure on the string is set up, the order parameters of each state are input as initial value in the SCFT followed by iteration steps. After certain iterations, the equal arc length limit is applied to the string by cubic spline interpolation mentioned above. Constant iteration and adjustment of the string were applied until it finally converges to the MEP on which each point is a metastable phase that may appear on the transition pathways between the initial phases M and N .

Initial Fields and Unit Cell Parameters Setting. There are numerous metastable phases due to the anisotropic orientation interaction and the geometrical asymmetry between rods and coil blocks in the rod–coil system. These metastable phases are very sensitive to the setting of initial fields and unit cell parameters in the SCFT calculations. Different initial fields may directly lead to different metastable or stable phases that correspond to an optimum unit cell size, and larger or smaller unit cell size will increase the overall free energy of the system. Here, we construct the initial field through real space,⁶⁷ using the strong segregation boundary (namely infinitely sharp) between two adjacent phase domains, where the concentration is set to 0 or 1. In this way, we can obtain various candidate phases according to the symmetry of target phases. Finally, all candidate phases are brought into the SCFT calculations with multiple sets of iterative operations to obtain the converged solution. Moreover, to reduce the confinement effect of computational cell size, a series of the unit cell size is performed to each candidate state to find the free energy corresponding to the optimal unit cell size, that is, the minimum free energy F_{\min} of the candidate phase under the parameter condition. By comparing F_{\min} among all candidate phases, the phase with the smallest F_{\min} is the most stable at the selected parameter, and the remaining candidate phases are all metastable structures in the free energy landscape.

RESULTS AND DISCUSSION

Various experiments have focused on the self-assembled structures of block copolymers with rigid chains due to their potential applications in organic optoelectronics.³⁴ But three-dimensional self-assembled structures of rigid rods and semiflexible block copolymers are still relatively undeveloped theoretically,^{50,68} which mainly focused on the study of lamellae,⁶⁹ the self-assembly behavior without orientation interactions⁶⁸ and theoretical calculation of the liquid crystal behavior under two-dimensional conditions.⁷⁰ One of the key factors behind this gap is the existence of the orientation interaction and the geometrical asymmetry between the rigid and flexible blocks, which makes numerical solution difficult to resolve or extremely unstable. The orientation interaction drives the rigid or semirigid blocks to be arranged in parallel along a specific direction, resulting in liquid crystal behavior, which becomes more prominent in the case of larger orientation interactions. Furthermore, the geometrical asymmetry between rods and coil blocks leads to the formation of large packing frustration in the rod–coil system. As a result, there is no complete study on the phase diagram and metastable phases for the rod–coil system so far, which is important for studying the transition mechanism between different phases.

According to the method of initial fields and unit cell parameters setting in **Theory and Computation Methods**, we consider the body-centered cube sphere (BCC), A15 phase (simple Frank–Kasper structure), hexagonal packed cylinders,

tetragonally packed cylinders, double gyroid phase (DG), and lamellae as candidate phases for our calculations. Based on the precision of $\chi N = 0.1$ and $f = 0.05$, the rod–coil phase diagram of $\chi N - f$ under $\beta = 2$ and $\mu N = 10$ is calculated, as shown in Figure 2, where G represents the double gyroid phase, C represents the

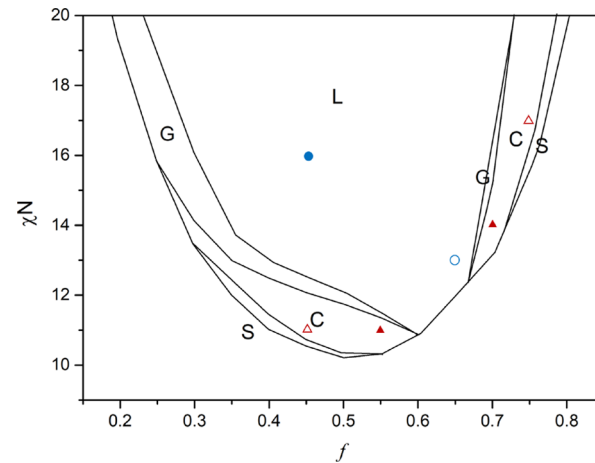


Figure 2. $\chi N - f$ phase diagram of the rod–coil system under $\beta = 2$ and $\mu N = 10$ based on the precision of $\chi N = 0.1$ and $f = 0.05$, and the data points for calculating the phase boundary are omitted to make the phase diagram clearer. The blue bold dot represents the parameter near the cylinder–lamella phase transition point and the blue hollow dot represents the parameter near the disorder–lamella phase transition point. The red bold triangles represent the parameter near the disorder–cylinder phase transition point and the red hollow triangles represent the parameter near the sphere–cylinder phase transition point.

hexagonal packed cylinder, S represents the simple spherical phase, and L represents the lamellar phase. We drop off the data points for calculating the phase boundary to make the phase diagram clear.

Rod–coil block copolymers differ from the coil–coil blocks in the orientation interaction and the geometrical asymmetry both of which cause the shape of phase diagram to change. Instead of the perfect symmetrical phase diagram of the coil–coil diblocks, the disorder–lamella transition point in the phase diagram is moved from the coil volume fraction $f = 0.5$ to a range between $f = 0.6$ and $f = 0.65$, which is also consistent with previous studies about the effect of orientation interactions and the geometrical asymmetry on the phase behavior of the rod–coil system.^{52,68,71,72} From $\chi N - f$ phase diagram of rod–coil blocks in the case of low-orientation interaction, we can see that a double continuous network structure DG appears in spite of complicated structures caused by the geometrical asymmetry and the orientation interaction. In the part of $f \leq 0.6$, with the increase of the rigid composition, the proportion of DG in the phase diagram is larger, which is in sharp contrast to the coil–coil system.³³ The main reason behind this phenomenon is the packing frustration. When complex networks formed, the excessive stretching caused by packing frustration is alleviated because the rods have less conformational entropy loss,³³ which is beneficial for the formation of complex network structures. In the phase diagram as shown in Figure 2, most of the area is still occupied by the lamellae and the cylinders, which is consistent with our previous findings.⁵²

Masten have found that in the process of the phase transition between different phases, there will be a specific epitaxial growth

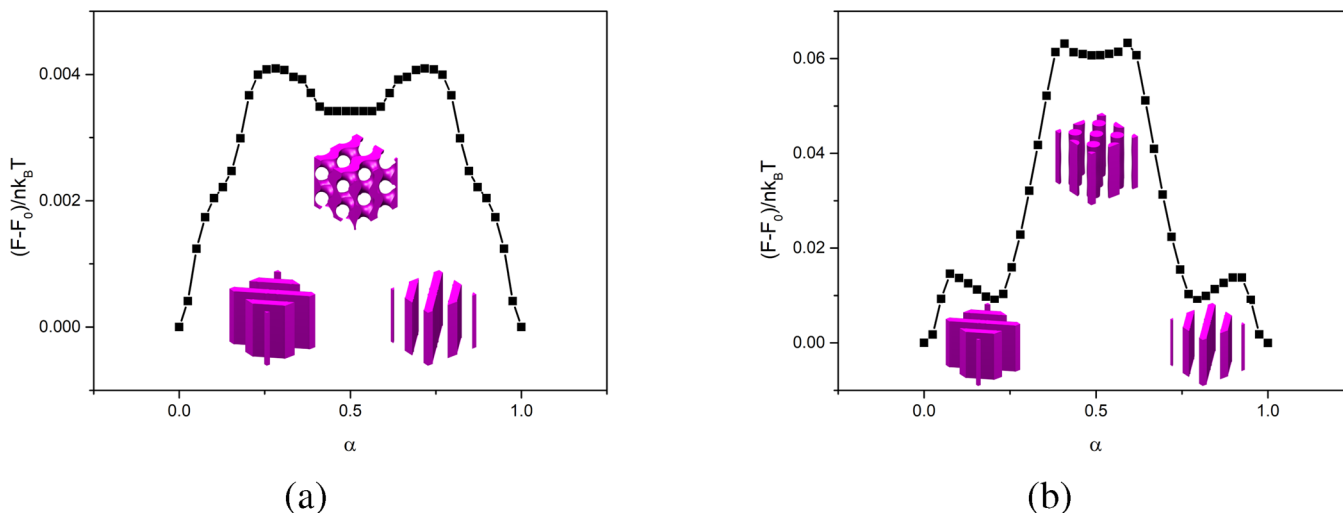


Figure 3. (a) Reordering transition pathway between $\{110\}$ lamellae in the rod–coil block copolymers with SG being encountered under $f = 0.65$, $\chi N = 13$, $\beta = 2$, and $\mu N = 10$ (b) and with tetragonally packed cylinders being encountered under $f = 0.45$, $\chi N = 16$, $\beta = 2$, and $\mu N = 10$.

relationship.^{73,74} Wang et al. also found that the epitaxial relationship originates from the matching of the dominant Fourier components of the structures.⁷⁵ According to our previous study on applying the string method to explore the phase transition pathway and the free-energy barrier of critical nuclei, the transition difficulty and occurrence of metastable phases are closely related to the epitaxial growth relationship between initial phases.^{51,64,76} When the space symmetry group and reciprocal lattice vectors are well matched, a small-scale adjustment occurs in the transition process, resulting in the phase transition being easy to achieve. Different self-assembled phases can belong to the same space group, but different phases with the same space group are usually distinguished by the reciprocal lattice vector with the strongest signal, that is, the main peak in the light scattering experiment.⁷⁷

In experiments, continuous annealing can realize the reordering transition between lamellae or cylinders with different orientations.⁷⁸ In the film-confined system, the phenomenon that lamellae or cylinders with different orientations coexist has been observed,⁷⁹ which is expected to be more complex in three-dimensional space. Here, we use crystallographic planes and crystallographic directions to denote the orientations of the lamellar and cylindrical phases.⁶⁴ Crystallographic planes and crystallographic directions are represented by three integers h , l , and k , namely, the Miller indices.⁸⁰ According to our previous work,⁵¹ the rearrangement transition pathway between different orientation lamellae of $\{110\}$ and $\{111\}$ crystallographic plane group at the parameters of $f = 0.65$, $\chi N = 13$, $\beta = 2$, and $\mu N = 13$ was investigated, and single gyroid (SG) and single diamond (SD) phases were found as the metastable structures. Combined with the phase diagram of rod–coil block copolymers, we find that single network phases appear around the disorder–lamella phase transition point. To confirm this, namely the influence of the selected location in the phase diagram on the reordering transition pathway, we study the rearrangement transition pathway between $\{110\}$ lamellae with different orientations at the disorder–lamella phase transition point and the cylinder–lamella phase transition point, which correspond to $f = 0.65$, $\chi N = 13$, $\beta = 2$, and $\mu N = 10$ and $f = 0.45$, $\chi N = 16$, $\beta = 2$, and $\mu N = 10$, respectively. The exact position of these parameters in the phase diagram is shown as the blue hollow and bold dots in

Figure 2, where the blue hollow dot identifies the point near disorder–lamella phase transition and the blue bold dot represents the point near cylinder–lamella phase transition.

As shown in Figure 3, it is found that in the reordering transition pathway of $\{110\}$ lamellae with different orientations, the SG appears under the parameter of $f = 0.65$, and the tetragonally packed cylinder occurs under the parameter of $f = 0.45$ instead of SG. According to the research on applying spatial symmetry group theory to the SCFT by Jiang et al.,⁷⁷ both SG and the tetragonally packed cylinder belong to the same epitaxial growth relationship of the $\{110\}$ crystallographic plane group. In addition, we find that the metastable phases appearing in the reordering transition pathway of different orientation $\{110\}$ lamellae tend to form the structure at the low χN side of the phase boundary comparing to lamellae. For example, cylinders appear in the rearrangement transition near the cylinder–lamella phase transition point, while SG appears near the disorder–lamella phase transition point. It was reported that the disorder phase can be described as a set of complex network structures.^{81,82} It is anticipated that in the rearrangement transition of different orientation lamellae, the metastable phases are related to the epitaxial growth relationship of initial lamellae and the selected parameter location in the phase diagram. Therefore, if we want to get SG structures, we can design a reordering pathway between lamellae with the same epitaxial growth relationship of SG, and parameters should be selected around the disorder–lamellae boundary.

To further determine if this relationship merely occurs in the lamellar phase rearrangement transition, near the sphere–cylinder ($f = 0.45$, $\chi N = 11$ and $f = 0.75$, $\chi N = 17$) and disorder–cylinder phase transition points ($f = 0.55$, $\chi N = 11$ and $f = 0.7$, $\chi N = 14$) on both sides of the disorder–lamella phase transition point with same $\beta = 2$ and $\mu N = 10$, we calculate the reordering transition pathways of different orientation cylinders with $\langle 111 \rangle$ crystallographic direction using the string method, as shown in Figure 4, where red structures represent the change of the coil blocks and blue structures indicate the change of the rigid blocks. It is found that the results are in good agreement with our expectations. BCC with rods as the minority domain appears in the rearrangement transition pathway between $\langle 111 \rangle$ cylinders at $f = 0.75$ and with coil segments as the minority domain at $f = 0.45$. Similarly, PL with rods and flexible

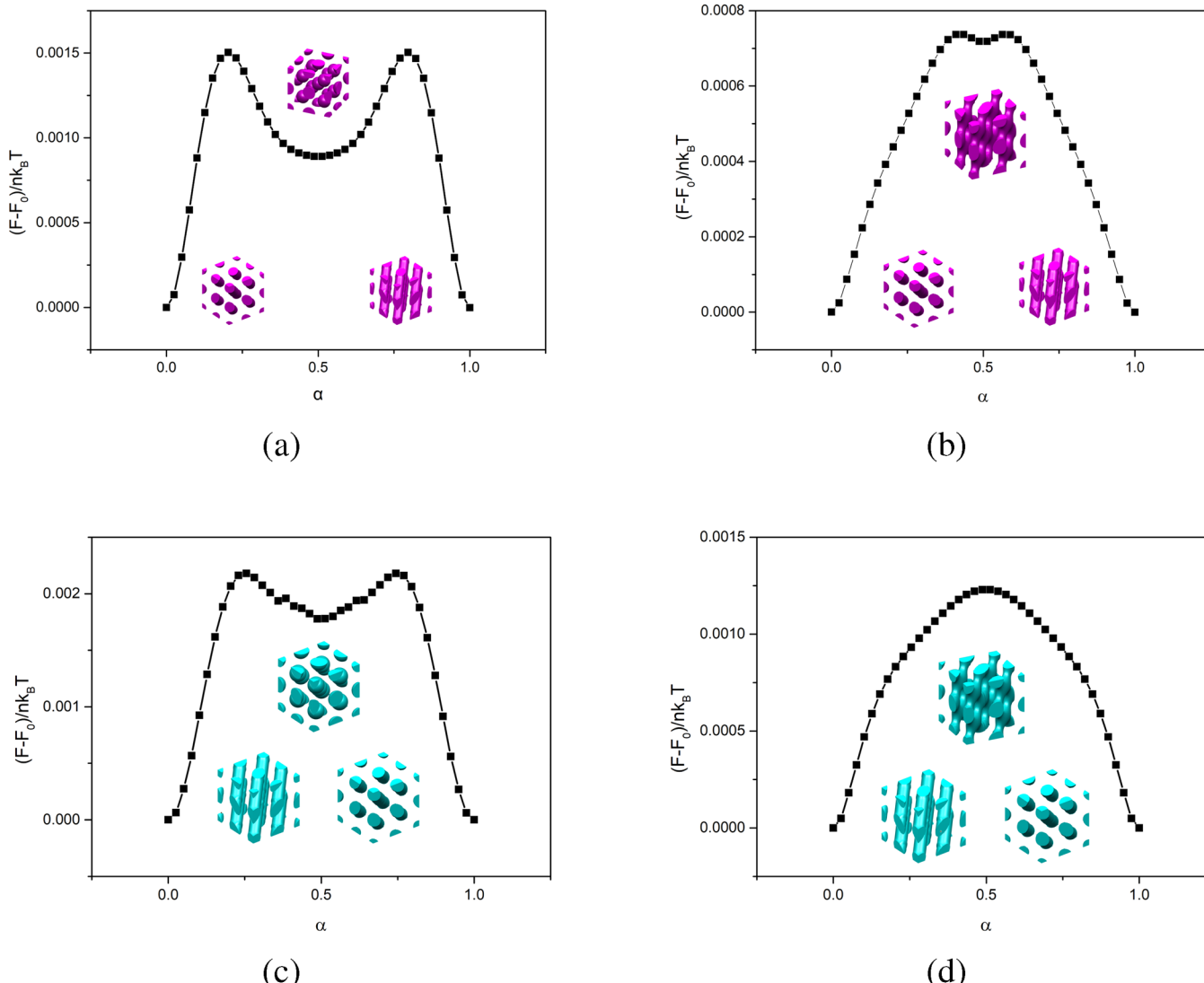


Figure 4. Reordering transition pathways between $<111>$ cylinders with BCC being encountered in the rod–coil block copolymers under (a) $f = 0.45$, $\chi N = 11$, and $\beta = 2$ and (c) $f = 0.75$, $\chi N = 17$, and $\beta = 2$. Reordering transition pathways between $<111>$ cylinders with PL being encountered in the rod–coil block copolymers under (b) $f = 0.55$, $\chi N = 11$, and $\beta = 2$ and (d) $f = 0.7$, $\chi N = 14$, and $\beta = 2$. The red structures in (a) and (b) represent the density of coil segments, and the blue structures in (c) and (d) represent the density of rigid blocks. Parameters of four reordering transitions are in Figure 2, represented by bold and hollow triangles.

segments as the minority domain respectively appears at $f = 0.7$ and $f = 0.55$. Compared with the lamellar phase, the concentration distribution of cylinders is too dispersive with more independent domains. Therefore, it is more difficult to form SG in the rearrangement transition pathway of $<111>$ crystallographic direction cylinders. At $f = 0.7$, PL with rod blocks as the minority domain is unstable, and it is easy to transform into a lamellar structure in the manner of spinodal. However, even if SG does not appear, PL still has some characteristics of complex network structures, which has the same epitaxial growth relationship of the $<111>$ crystallographic direction. Obviously, the result also shows that the above conclusion is not only applicable to the lamellar phase but also to the cylindrical phase rearrangement transition both of which occupy the most area of the phase diagram in the rod–coil system and are easy to be obtained.

We believe that the mechanism for this kind of transformation is that the system has undergone the process of distortion, fracture, and reorganization during the rearrangement transition

of cylinders and lamellae with different orientations. The symmetry of initial phases is destroyed in the reordering transition and thus the system tends to form morphologies with large entropy and high interface area. To further understand this mechanism, we analyze the corresponding changes of the entropy $-\frac{S}{nk_B T}$ (eq 2), the contacting degree between rods and coil segments $\frac{F'}{nk_B T}$, and the average orientation degree of rods M .

Here, we use the order parameter $\tilde{S}(\mathbf{r}) = 3/2 \times \lambda_{\max}(\mathbf{r})$ to indicate the degree of orientation, and the average orientation degree of rods is defined as $M = \int \tilde{S}(\mathbf{r}) dV_{\text{rod}} / V_{\text{rod}}$, where V_{rod} is the domain volume of rods and $\lambda_{\max}(\mathbf{r})$ represents the maximum eigenvalue of matrix tensor $\mathbf{S}(\mathbf{r})$.⁵³ The degree of contacting between rods and coil segments $\frac{F'}{nk_B T}$ can be defined as⁸¹

$$\frac{F'}{nk_B T} = \partial \left(\frac{F'}{nk_B T} \right) / \partial (\chi N) = \int d\mathbf{r} \phi_A(\mathbf{r}) \phi_B(\mathbf{r}) / V \quad (8)$$

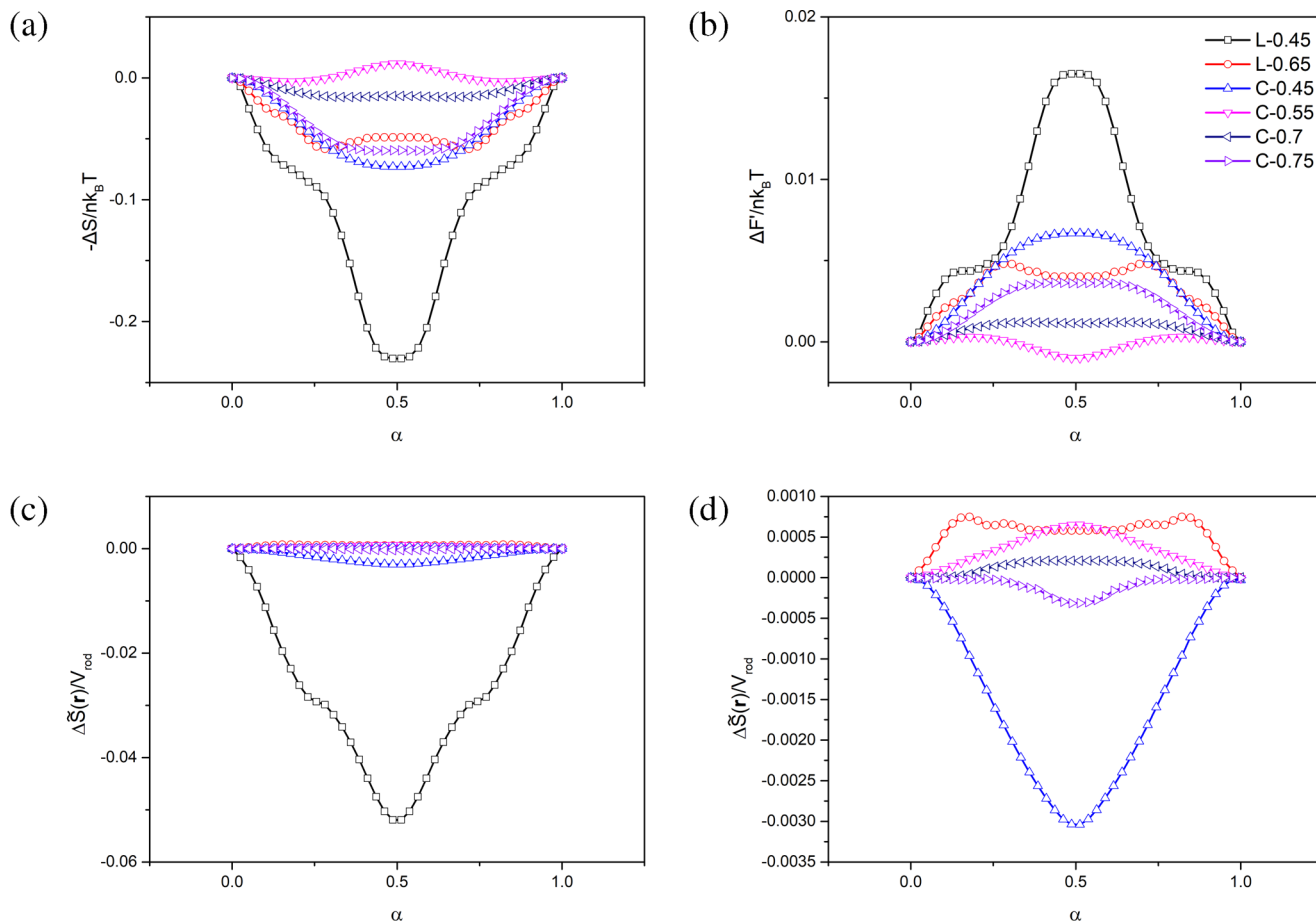


Figure 5. (a) Changes in $-\frac{s}{nk_B T}$ along the string during the rearrangement transition. (b) Changes in $\frac{F'}{nk_B T}$ during the reordering transition. (c) Changes in M during the reordering transition and (d) magnification of the variation of the five small-amplitude average orientation degrees in (c).

The above parameters are plotted against the string contour parameter α , as shown in Figure 5; squares and circles indicate the changes in the rearrangement transition pathway of {110} lamellae with different orientations under $f = 0.45$ and $f = 0.65$, which are represented by transition I and transition II, respectively. The remaining triangles represent the changes in the rearrangement transition pathway of <111> crystallographic direction cylinders under $f = 0.45$, $f = 0.55$, $f = 0.7$, and $f = 0.75$ and are expressed as transition III to transition VI. It can be seen from Figure 5a that in most cases, the total entropy of systems increases in the reordering transition pathway. Interestingly, when a complex network structure appears in the transition such as SG in the transition II and PL in the transitions IV and V, the entropy of systems decreases in the rearrangement transition pathway. This phenomenon occurs mainly because the complex network structure has large packing frustration, and its entropy stretching directly leads to more entropy loss of the system.³³ Nevertheless, the rigid block itself in the rod–coil system has no conformational entropy, so the entropy loss caused by this entropy stretching is alleviated, and complex network structures still appear in the transition. Figure 5b shows the changes in the degree of contacting between rods and coil blocks during the six rearrangement transitions. It is similar to Figure 5a that the degree of contacting increases in most transitions but slightly decreases in the transitions II, IV, and V where the complex network structures appear. With the entropy stretching caused by packing frustration increasing, the extent of interpenetration

between coil blocks and rigid blocks decreases and thus reducing the contacting degree between rods and coils.

From Figure 5c,d, the trend of average orientation degree in the six rearrangement transitions can be obtained. It is clear that the changes of the average orientation degree are small, where the change in the transition I is one order of magnitude smaller than the change in its entropy, and even worse, the rest of the rearrangement transitions are three or four orders of magnitude smaller than the change in their entropy. To ensure the numerical stability during the calculation process, we choose a smaller μN , which leads to a smaller orientation degree of rods, but even so, the rod blocks still maintain a certain degree of parallel arrangement, as shown in Figure 6. Although the variation of the average orientation degree is small, its changes are very interesting. Similar to the change in the entropy and the degree of contacting between rods and coil segments, the average orientation degree of transitions I, III, and VI decreases in the reordering transition, which leads to a raise in free energy, indicating that the rod blocks tend to be chaotically arranged and the system tends to increase the orientation entropy during the rearrangement transition. Although the average orientation degree of transitions II, IV, and V increases during the rearrangement transition, which is the same as special changes in the entropy and the degree of contacting, we believe that this change is related to the complex network structure that emerges in the transition. To illustrate this, we have drawn the three-dimensional structure of metastable complex networks in

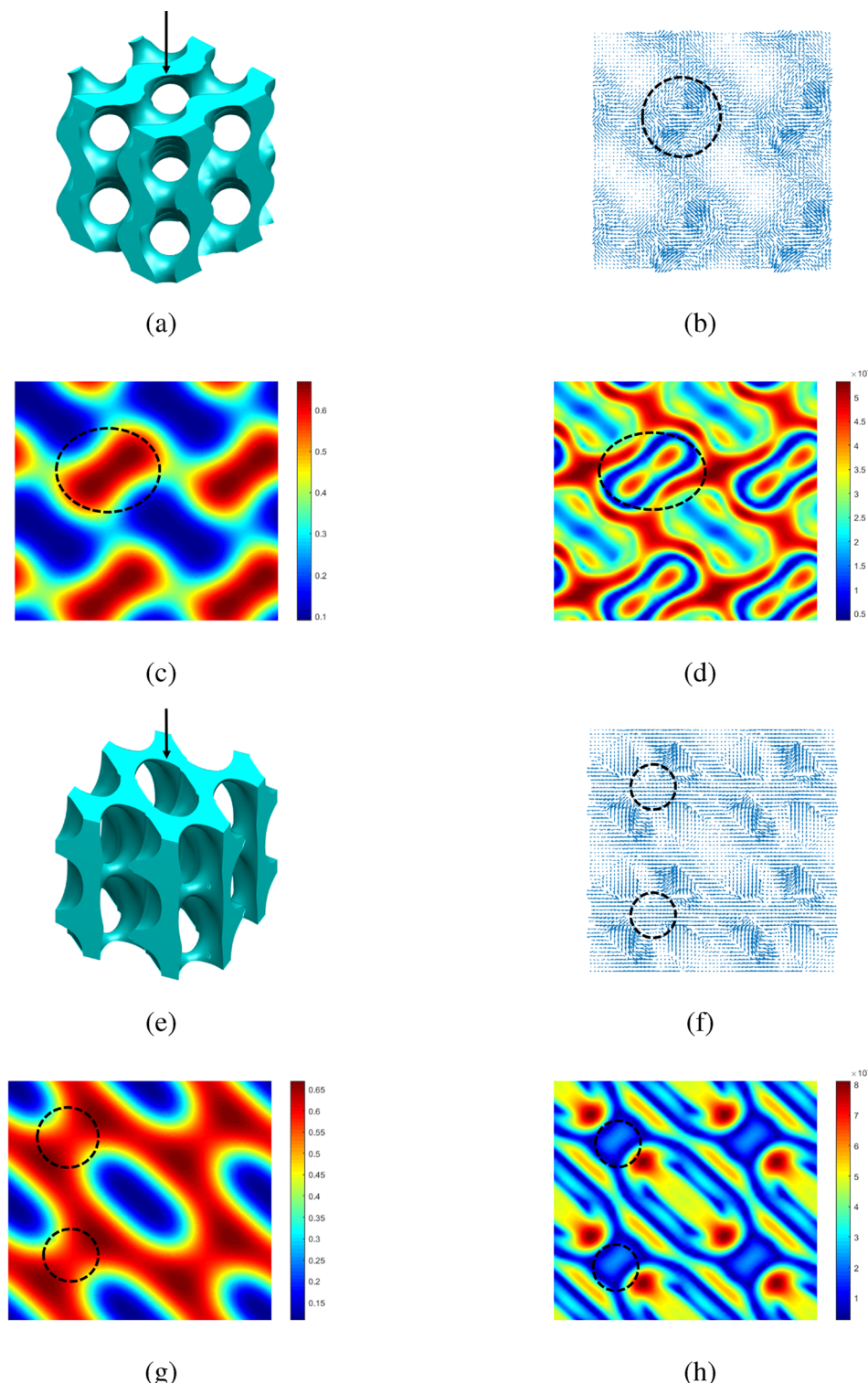


Figure 6. (a) Three-dimensional structure of the complex network structure. (b) Visual orientation tensor field $S(\mathbf{r})$ of the rods in two dimensions, along the direction of the arrow in (a). (c) Concentration distribution and (d) orientation degree of rods in two dimensions, which has the same direction as (b). (a), (b), (c), and (d) are SG in the reordering transition pathway between $\{110\}$ lamellae at $f = 0.65$, $\chi N = 13$, $\beta = 2$, and $\mu N = 10$. (e), (f), (g), and (h) represent the same content as (a), (b), (c), and (d) but are PL in the reordering transition pathway between $<111>$ crystallographic direction cylinders at $f = 0.55$, $\chi N = 11$, $\beta = 2$, and $\mu N = 10$. The black dotted lines are the network nodes.

transitions II and IV, two-dimensional visual orientation tensor field of rod blocks along the Z axis direction $S(\mathbf{r})$, the concentration and the orientation degree distribution map of rods, as shown in Figure 6. We use the order parameter $\tilde{S}(\mathbf{r})$ to indicate the degree of orientation, and the black dotted lines in

the figures show the location of nodes in complex network structures, where the orientation degree of rods is lower. From Figure 6b,f, we can find that rod blocks from different branches converge at nodes with different orientations, which results in a disorder orientation state of rods at nodes. The complex

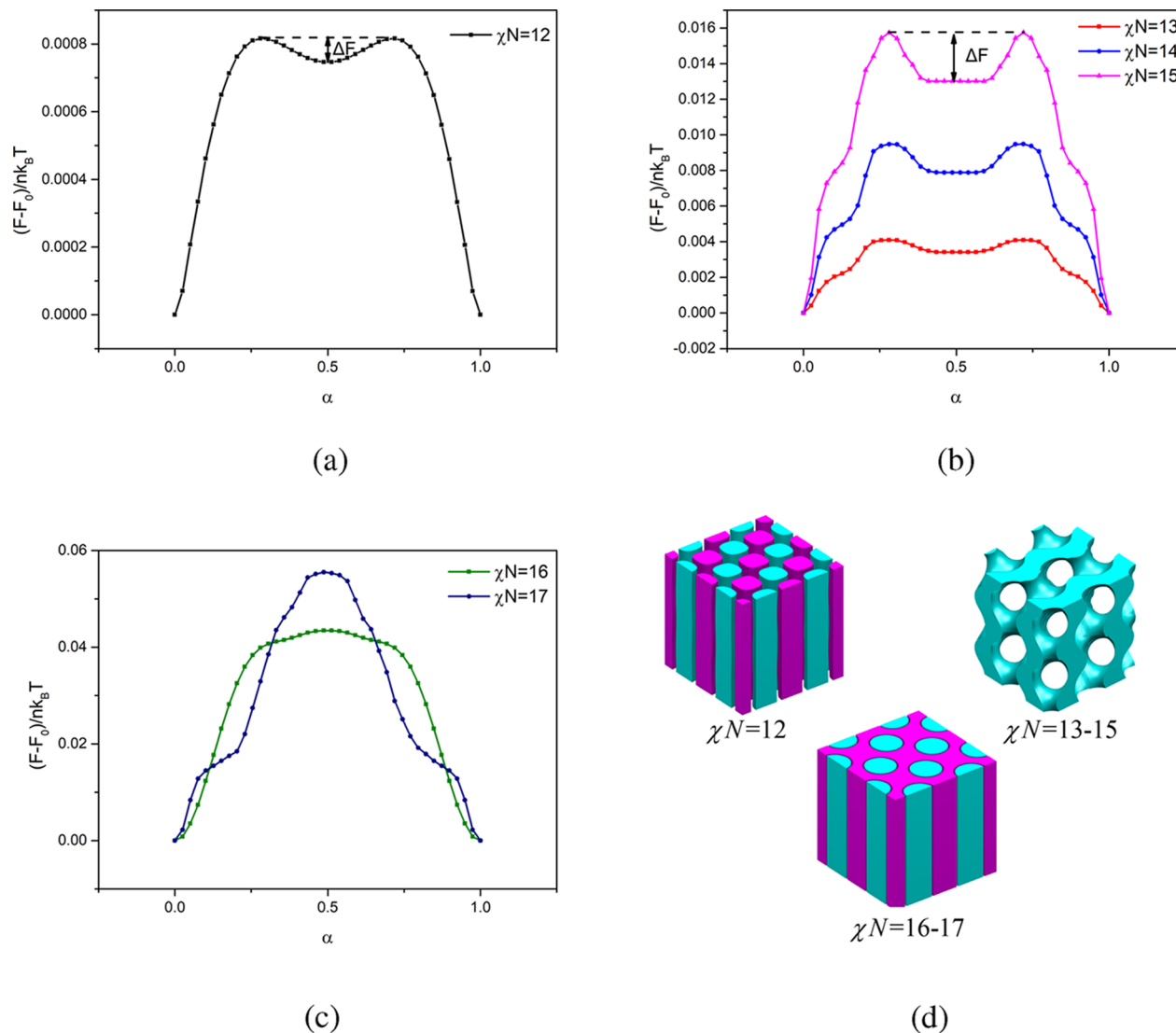


Figure 7. (a–c) Changes of the singe-chain free energy during the reordering transition pathways of {110} lamellae with different orientations from $\chi N = 12$ to $\chi N = 17$ in the condition of $f = 0.65$, $\beta = 2$, and $\mu N = 10$. (d) Structures at $\alpha = 0.5$ in (a–c) to represent the metastable phases appearing in the reordering transition pathways, which are two kinds of tetragonally packed cylinders with low and high segregation and SG.

network phase has a high packing frustration, which leads to the entropy stretching of rod blocks.³³ Furthermore, this entropy stretching process is beneficial to the ordered parallel arrangement of rod blocks without conformational entropy, thus increasing the orientation degree of rods around nodes. So, this special behavior in the rod–coil system can alleviate the entropy loss in complex network structures, which is consistent with our conclusion that the orientation interaction of rod blocks is at some extent beneficial to the formation of complex network structures in the rod–coil phase diagram.

As analyzed above, we can see that metastable phases appearing in the reordering transition pathway are closely related to the structure at the low χN side of the phase boundary compared with initial phases. When the initial phases at both ends of the string are near the OOT (the initial phase is at the high χN side of the phase boundary), for example, near the sphere–cylinder transition point and the cylinder–lamella transition point, the entropy and the degree of blending between rods and coil blocks in the rod–coil block copolymer increase in the reordering transition pathways between cylinders or lamellae with different orientations, and the metastable phase tends to

form the sphere and cylinder. When initial phases are near the order–disorder transition (ODT), the metastable phases in the reordering transition pathway will form complex network structures that can be used to describe the disorder phase.⁸¹ Unlike the coil–coil system, due to the special existence of rods, the orientation interaction and the nonconformational entropy of rod–coil can alleviate the packing frustration of complex network structures, which makes the complex networks composed of the rod–coil block copolymer easier to be discovered in experiments. Moreover, the rod–coil system has higher selectivity for experimental conditions, and the complex networks formed with rods have applications in the fields of 3D photonic crystals and the like.

We need to consider the scope of application after understanding the mechanism of the reordering transition, including the parameter and the chemical components, to determine whether there is a higher practical value. So, taking {110} lamellae rearrangement transition under $f = 0.65$, $\beta = 2$, and $\mu N = 10$ as an example, we calculate a series of reordering transitions with χN changing from 12 to 17, as shown in Figure 7 and Table 1. Two characteristic free energy barriers are defined

Table 1. Effect of χN in the Rod–Coil System on Long-Term Stability of Intermediate Structures in {110} Lamellae Phase Transition Pathways

Flory–Huggins interaction parameter (χN)	intermediate structure ($\alpha = 0.5$)	$F_1/k_B T$	$\Delta F/k_B T$
12	tetragonally packed cylinders with low segregation	0.00082	0.00007
13	SG	0.00409	0.00067
14	SG	0.00948	0.00159
15	SG	0.01573	0.00272
16	tetragonally packed cylinders	0.04345	not exist
17	tetragonally packed cylinders	0.05551	not exist

here. ΔF represents the single-chain free energy difference between the valley and the barrier in the rearrangement transition pathway. The larger ΔF means the longer stability of the metastable phase. In addition, F_1 indicates the single-chain free energy barrier in the rearrangement transition pathway that needs to be crossed to form a metastable structure in the transition, and a larger value of F_1 indicates more difficulties in the reordering transition, only when $\Delta F > 0.1 \times F_1$ do we think that the metastable phase has long-term stability. When χN is small and the lamella phase is metastable comparing with the disorder, represented by the result of $\chi N = 12$, the single-chain free energy barrier and the degree of segregation are low in {110} lamellae rearrangement transition pathway, and the blocks including rods and coils are largely intertwined to form tetragonally packed cylinders, which is not a long-lived structure according to the above standards for long-term stability, as shown in Figure 7d. When χN changes from 13 to 15, the complex bicontinuous network structure SG appears with long-term stability, whose single-chain free energy barrier F_1 , single-chain free energy difference ΔF , and long-term stability all increase with χN . We can see that ΔF is only $10^{-3} k_B T$ for SG from Table 1, but ΔF is the single-chain free energy difference and the total energy difference of the system needs to multiply the number of molecular chains. Therefore, this barrier is relatively large, thus easily maintaining the metastable state experimentally. The packing frustration of the system will increase with χN ,³³ and when χN exceeds 15, represented by the results of $\chi N = 16, 17$, the extremely high interactions make the packing frustration of SG exceed its critical value, resulting in F_1 increasing sharply. At this moment, ΔF no longer exists, and tetragonally packed cylinders form without long-term stability. According to the above discussions, the mechanism of the reordering transition is suitable for a broad parameter space, which is very beneficial for obtaining the desired complex network structure experimentally.

Under the condition that this mechanism is suitable for the most of parameters, we change the system to the coil–coil block copolymer to determine whether this mechanism is only applicable to the rod–coil block copolymer. According to the thoroughly studied phase diagram of the coil–coil block copolymers, we select the reordering transition pathway of {110} lamellae with $f = 0.5$ and $\chi N = 11$ and $f = 0.4$ and $\chi N = 15$ near disorder–lamella and cylinder–lamella transition boundaries, respectively. Also, the rearrangement transitions of <111> cylinders with $f = 0.3$ and $\chi N = 16$ and $f = 0.4$ and $\chi N = 12$ near sphere–cylinder and disorder–cylinder transition boundaries are drawn respectively. The exact position of these parameters in

the coil–coil phase diagram³³ is shown in Figure 8e. It can be seen from Figure 8 that SG appears in the rearrangement transition pathway of {110} lamellae near the disorder–lamella transition point and the tetragonally packed cylinder appears near the cylinder–lamella transition point. For the reordering transition pathways of <111> cylinders, the metastable phases near the sphere–cylinder and the disorder–cylinder transition boundary are BCC and PL, respectively. This is consistent with our previous results regarding the rod–coil block copolymer rearrangement transition and fully satisfied the conclusion that the metastable phases existing in the reordering transition are related to the epitaxial growth relationship and the selected parameter location in the phase diagram. This discovery is quite exciting because it breaks through the limit of the system and promotes the study on controlling phase transition pathways to achieve the fabrication of target structures.

For a better comparison with the rod–coil system and a deeper understanding of the mechanism of rearrangement transitions, we calculate the changes of single-chain entropy $-\frac{s}{nk_B}$ and the degree of contacting between segments $\frac{f'}{nk_B T}$ in four coil–coil reordering transitions mentioned above

$$-\frac{s}{nk_B} = \frac{1}{V} \int d\mathbf{r} \{-\omega_A(\mathbf{r})\phi_A(\mathbf{r}) - \omega_B(\mathbf{r})\phi_B(\mathbf{r}) - \eta(\mathbf{r})[1 - \phi_A(\mathbf{r}) - \phi_B(\mathbf{r})]\} - \ln Q \quad (9)$$

$$\frac{f'}{nk_B T} = \partial \left(\frac{f'}{nk_B T} \right) / \partial (\chi N) = \int d\mathbf{r} \phi_A(\mathbf{r})\phi_B(\mathbf{r}) / V \quad (10)$$

Similar to the rod–coil block copolymer, when a complex network phase appears in the rearrangement transition, the entropy and the degree of segments mixing decrease, as shown in Figure 9. The entropy and the segments mixing degree decrease in the reordering transitions with SG and PL being encountered, which is related to the packing frustration required by complex network structure formation. However, the segments contacting degree also has a little drop in other two reordering transitions pathways. This is because BCC and the cylinder still have a certain degree of packing frustration in the coil–coil block copolymer, which is alleviated by the orientation interaction of rods in the rod–coil system. The coil–coil block copolymer is simple with no orientation interaction μN and geometrical asymmetry parameter β and only has the interface energy and the entropy in the system to determine the final phase morphology. When a complex network forms, the entropy stretching produced by packing frustration makes the phase domain tends to be uniform in thickness, and the interfacial energy acts to minimize the domain area, which favors uniform interfacial curvature.³³ The competition between the tendency for uniform curvature and uniform domain thickness will result in final phase morphologies, and the entropy stretching will cause the entropy loss in the coil–coil system. From the above discussions, it is clear that the mechanism of rearrangement transitions also has a well universality for coil–coil block copolymers, and this provides hope for fabricating various target structures by controlling the rearrangement transition in experiments.

CONCLUSIONS

We have studied on achieving constructing the target structure via designing phase transition pathways and promoted the

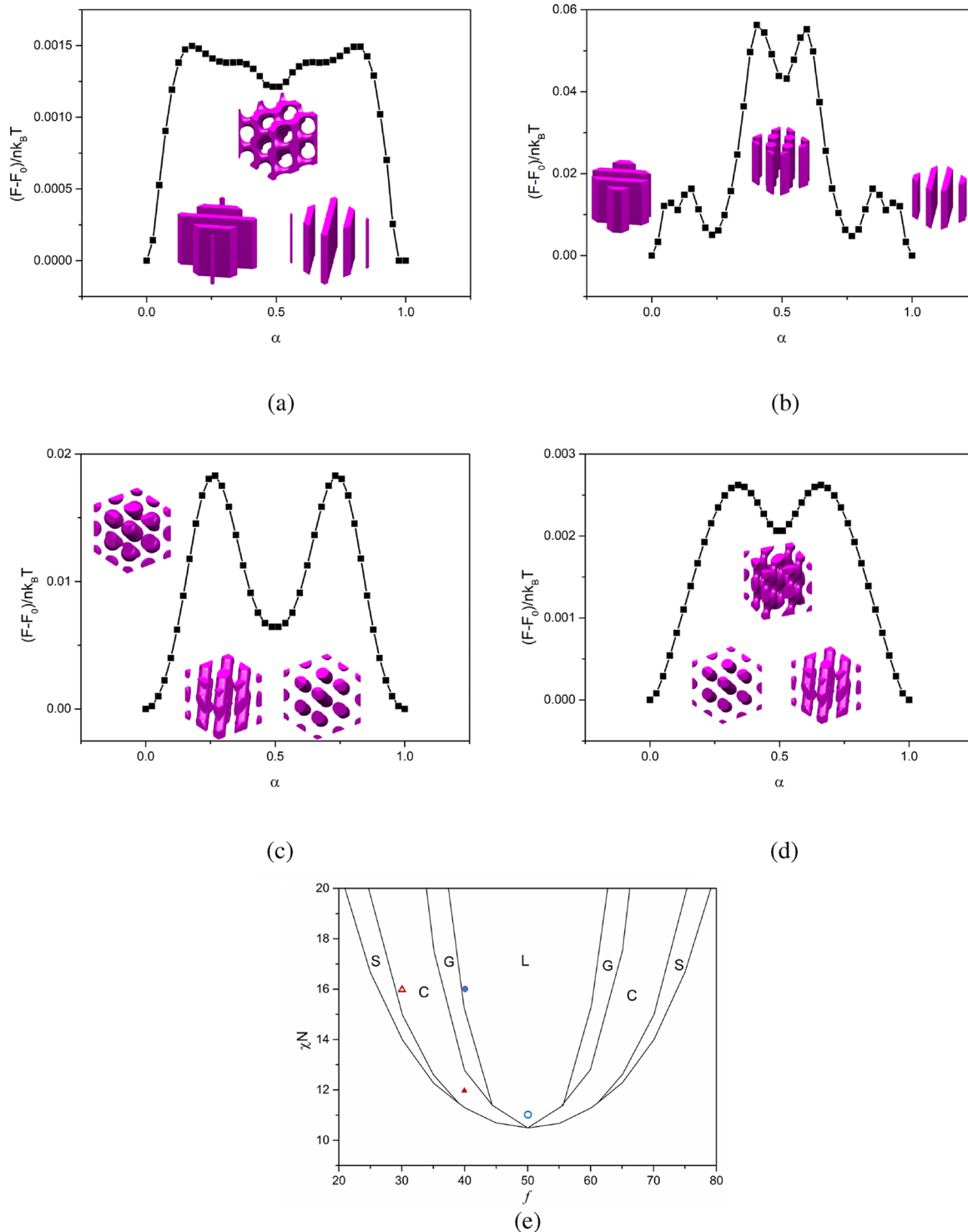


Figure 8. (a) Reordering transition pathways between $\{110\}$ lamellae in the coil–coil system with SG being encountered under $f = 0.5$ and $\chi N = 11$ and (b) with tetragonally packed cylinders being encountered under $f = 0.4$ and $\chi N = 16$. (c) Reordering transition pathways between $<111>$ cylinders in the coil–coil system with BCC being encountered under $f = 0.3$ and $\chi N = 16$ and (d) with PL being encountered under $f = 0.4$ and $\chi N = 12$. (e) Phase diagram of the coil–coil system that has been studied before.³³ The blue bold and hollow dots represent the parameter near the cylinder–lamella phase transition point and the disorder–lamella phase transition point, respectively. The red bold and hollow triangles represent the parameter near the disorder–cylinder phase transition point and the sphere–cylinder phase transition point, respectively.

development of the existing phase transition theory. The metastable phases appearing in the rearrangement transition pathways are determined by the matching degree of the dominant Fourier components, unit cell size, and selected parameter location in the phase diagram. The metastable phase

appearing in the reordering transition pathway tends to form the structure at the low χN side of the OOT boundary compared with the initial phase. In particular, for complex network metastable structures (SG, PL, etc.), it is necessary to select a rearrangement transition between lamellae or cylinders near the

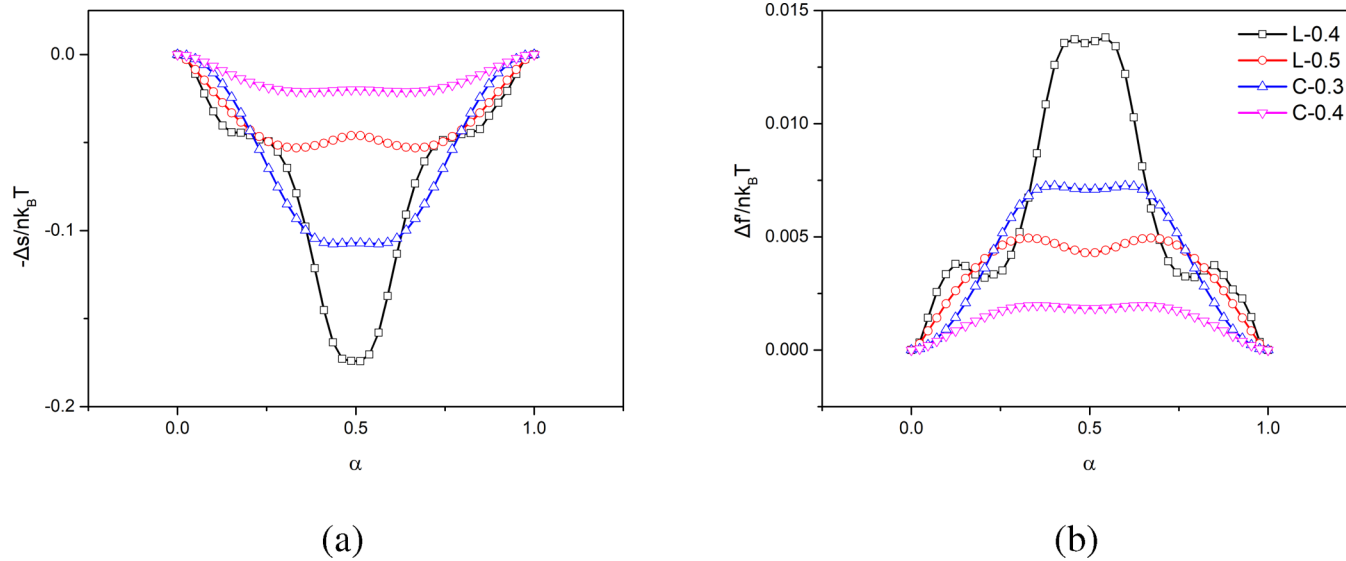


Figure 9. Changes of (a) single-chain entropy $-\frac{s}{nk_B T}$ and (b) degree of contacting between segments $\frac{f'}{nk_B T}$ in four reordering transition pathways of the coil–coil systems above, where the representation of each line is shown in the inset of (b).

ODT boundary with the same epitaxial growth relationship but different orientations. Combined with the phase diagram of the rod–coil system, epitaxial growth relationship, and mechanism of reordering transitions, we can completely achieve the fabrication of target phases by controlling the rearrangement transition pathways. For instance, if we want to get SG structures in experiments, we should design a reordering pathway between {110} lamellae around the disorder–lamellae boundary. According to our conclusions and the relevant phase diagram, we can determine the parameters that can be easily obtained in practical of the reordering pathway. Then, we can use solvent vapor annealing and field methods⁸³ to reorder {110} lamellae in experiments to get SG.

We also analyze the free energy, entropy, mixing degree between different blocks, and orientation degree during the rearrangement transitions of the rod–coil block copolymer and compare those with the coil–coil block copolymer. It is found that the entropy stretching caused by packing frustration of the complex network structures during rearrangement transitions makes the entropy and the blocks mixing degree decrease, which is advantageous for the parallel orientation of rod blocks and beneficial to alleviate the packing frustration from complex networks, so the rod–coil system has natural advantages for constructing complex network structures.

Finally, we validate that this rearrangement transition mechanism can be applied to a wide range of χN , as well as the coil–coil block copolymer. Thus, it is beneficial to experimentally obtain target structures, improving guidance for the synthesis of block copolymers and the preparation of self-assembly structures. We hope that this study can contribute to the material design of the rod–coil system experimentally via controlling kinetic routes.

AUTHOR INFORMATION

Corresponding Author

*E-mail: pingtang@fudan.edu.cn.

ORCID

Ping Tang: [0000-0003-0253-1836](#)

Notes

The authors declare no competing financial interest.

ACKNOWLEDGMENTS

The authors acknowledge financial support from the National Natural Science Foundation of China (grant nos. 21574027, 21774027, and 21534002).

REFERENCES

- Inoue, T.; Soen, T.; Hashimoto, T.; Kawai, H. Thermodynamic interpretation of domain structure in solvent-cast films of A-B type block copolymers of styrene and isoprene. *J. Polym. Sci., A-2 Polym Phys* **1969**, *7*, 1283–1301.
- Williams, D. R. M.; Fredrickson, G. H. Cylindrical micelles in rigid-flexible diblock copolymers. *Macromolecules* **1992**, *25*, 3561–3568.
- Leibler, L. Theory of microphase separation in block copolymers. *Macromolecules* **1980**, *13*, 1602–1617.
- Matsen, M. W.; Schick, M. Stable and unstable phases of a diblock copolymer melt. *Phys. Rev. Lett.* **1994**, *72*, 2660–2663.
- Matsen, M. W.; Bates, F. S. Block copolymer microstructures in the intermediate-segregation regime. *J. Chem. Phys.* **1997**, *106*, 2436–2448.
- Tang, P.; Qiu, F.; Zhang, H.; Yang, Y. Morphology and phase diagram of complex block copolymers: ABC linear triblock copolymers. *Phys. Rev. E: Stat., Nonlinear, Soft Matter Phys.* **2004**, *69*, No. 031803.
- Arora, A.; Pillai, N.; Bates, F. S.; Dorfman, K. D. Predicting the phase behavior of ABAC tetrablock terpolymers: sensitivity to flory-huggins interaction parameters. *Polymer* **2018**, *154*, 305–314.
- Gao, J.; Tang, P.; Yang, Y. Non-lamellae structures of coil-semiflexible diblock copolymers. *Soft Matter* **2013**, *9*, 69–81.
- Patterson, A. L.; Danielsen, S. P. O.; Yu, B.; Davidson, E. C.; Fredrickson, G. H.; Segalman, R. A. Sequence effects on block copolymer self-assembly through tuning chain conformation and segregation strength utilizing sequence-defined polypeptoids. *Macromolecules* **2019**, *52*, 1277–1286.
- Tang, P.; Qiu, F.; Zhang, H.; Yang, Y. Morphology and phase diagram of complex block copolymers: ABC star triblock copolymers. *J. Phys. Chem. B* **2004**, *108*, 8434–8438.
- Levi, A. E.; Lequeieu, J.; Horne, J. D.; Bates, M. W.; Ren, J. M.; Delaney, K. T.; Fredrickson, G. H.; Bates, C. M. Miktoarm stars via

- grafting-through copolymerization: selfassembly and the star-to-bottlebrush transition. *Macromolecules* **2019**, *52*, 1794–1802.
- (12) Spencer, R. K. W.; Matsen, M. W. Field-theoretic simulations of bottlebrush copolymers. *J. Chem. Phys.* **2018**, *149*, 184901.
- (13) Matsen, M. W. Phase behavior of block copolymer/homopolymer blends. *Macromolecules* **1995**, *28*, 5765–5773.
- (14) Lin, Y.; Böker, A.; He, J.; Sill, K.; Xiang, H.; Abetz, C.; Li, X.; Wang, J.; Emrick, T.; Long, S.; Wang, Q.; Balazs, A.; Russell, T. P. Self-directed self-assembly of nanoparticle/copolymer mixtures. *Nature* **2005**, *434*, 55–59.
- (15) Lu, S.; Liu, T.; Ke, L.; Ma, D.-G.; Chua, S.-J.; Huang, W. Polyfluorene-based light-emitting rodcoil block copolymers. *Macromolecules* **2005**, *38*, 8494–8502.
- (16) Topham, P. D.; Parnell, A. J.; Hiorns, R. C. Block copolymer strategies for solar cell technology. *J. Polym. Sci., B: Polym. Phys.* **2011**, *49*, 1131–1156.
- (17) Sikkema, D. J. Design, synthesis and properties of a novel rigid rod polymer, PIPD or 'M5': high modulus and tenacity fibres with substantial compressive strength. *Polymer* **1998**, *39*, 5981–5986.
- (18) Liu, C.-L.; Lin, C.-H.; Kuo, C.-C.; Lin, S.-T.; Chen, W.-C. Conjugated rod-coil block copolymers: synthesis, morphology, photophysical properties, and stimuli-responsive applications. *Prog. Polym. Sci.* **2011**, *36*, 603–637.
- (19) Becker, S.; Ego, C.; Grimsdale, A. C.; List, E. J. W.; Marsitzky, D.; Pogantsch, A.; Setayesh, S.; Leising, G.; Müllen, K. Optimisation of polyfluorenes for light emitting applications. *Synth. Met.* **2001**, *125*, 73–80.
- (20) Xu, Y.; Zhang, F.; Feng, X. Patterning of conjugated polymers for organic optoelectronic devices. *Small* **2011**, *7*, 1338–1360.
- (21) Gernigon, V.; Lévéque, P.; Richard, F.; Leclerc, N.; Brochon, C.; Braun, C. H.; Ludwigs, S.; Anokhin, D. V.; Ivanov, D. A.; Hadzioannou, G.; Heiser, T. Microstructure and optoelectronic properties of P3HT-b-P4VP/PCBM blends: impact of PCBM on the copolymer self-assembly. *Macromolecules* **2013**, *46*, 8824–8831.
- (22) Zhong, K.; Chen, T.; Jin, L. Self-assembly of rod-coil molecules with poly(ethylene oxide) chains and phenylene rods. *Prog. Chem.* **2012**, *24*, 1353–1358.
- (23) Olsen, B.; Segalman, R. Self-assembly of rod-coil block copolymers. *Mater. Sci. Eng., R Rep* **2008**, *62*, 37–66.
- (24) Semenov, A. N. Smectic ordering in block-copolymer melts. *Mol. Cryst. Liq. Cryst.* **2006**, *209*, 191–199.
- (25) Lam, J. W. Y.; Kong, X.; Dong, Y.; Cheuk, K. K. L.; Xu, K.; Tang, B. Z. Synthesis and properties of liquid crystalline polyacetylenes with different spacer lengths and bridge orientations. *Macromolecules* **2000**, *33*, 5027–5040.
- (26) Chécot, F.; Rodríguez-Hernández, J.; Gnanou, Y.; Lecommandoux, S. PH-Responsive micelles and vesicles nanocapsules based on polypeptide diblock copolymers. *Biomol. Eng.* **2007**, *24*, 81–85.
- (27) Babin, J.; Rodriguez-Hernandez, J.; Lecommandoux, S.; Klok, H. A.; Achard, M. F. Self-assembled nanostructures from peptide-synthetic hybrid block copolymers: complex, stimuli-responsive rod-coil architectures. *Faraday Discuss.* **2005**, *128*, 179–192.
- (28) Zhuang, Z.; Cai, C.; Jiang, T.; Lin, J.; Yang, C. Self-assembly behavior of rod-coil-rod polypeptide block copolymers. *Polymer* **2014**, *55*, 602–610.
- (29) Klok, H. A.; Langenwalter, J. F.; Lecommandoux, S. Self-assembly of peptide-based diblock oligomers. *Macromolecules* **2000**, *33*, 7819–7826.
- (30) Song, W.; Tang, P.; Zhang, H.; Yang, Y.; Shi, A.-C. New numerical implementation of selfconsistent field theory for semiflexible polymers. *Macromolecules* **2009**, *42*, 6300–6309.
- (31) Gao, J.; Song, W.; Tang, P.; Yang, Y. Self-assembly of semiflexible block copolymers: 2D numerical implementation of self-consistent field theory. *Soft Matter* **2011**, *7*, 5208–5216.
- (32) Matsen, M. W.; Bates, F. S. Origins of complex self-assembly in block copolymers. *Macromolecules* **1996**, *29*, 7641–7644.
- (33) Matsen, M. W. The standard gaussian model for block copolymer melts. *J. Phys.: Condens. Matter* **2002**, *14*, R21.
- (34) Park, J. W.; Thomas, E. L. Multiple ordering transitions: hierarchical self-assembly of rodcoil block copolymers. *Adv. Mater.* **2003**, *15*, 585–588.
- (35) You, S.; Zhong, K.; Jin, L. Y. Control of supramolecular nanoassemblies by tuning the interactions of bent-shaped rod-coil molecules. *Soft Matter* **2017**, *13*, 3334–3340.
- (36) Cao, X.; Mao, W.; Mai, Y.; Han, L.; Che, S. Formation of diverse ordered structures in ABC triblock terpolymer templated macroporous silicas. *Macromolecules* **2018**, *51*, 4381–4396.
- (37) Werner, J. G.; Rodríguez-Calero, G. G.; Abruña, H. D.; Wiesner, U. Block copolymer derived 3D interpenetrating multifunctional gyroidal nanohybrids for electrical energy storage. *Energy Environ. Sci.* **2018**, *11*, 1261–1270.
- (38) Fruchart, M.; Jeon, S.-Y.; Hur, K.; Cheianov, V.; Wiesner, U.; Vitelli, V. Soft self-assembly of weyl materials for light and sound. *Proc. Natl. Acad. Sci. U. S. A.* **2018**, *115*, E3655–E3664.
- (39) Edwards, S. F. The Statistical mechanics of polymers with excluded volume. *Proc. Phys. Soc.* **1965**, *85*, 613–624.
- (40) Bates, C. M.; Bates, F. S. 50th Anniversary perspective: block polymers-pure potential. *Macromolecules* **2016**, *50*, 3–22.
- (41) Foerster, S.; Khandpur, A. K.; Zhao, J.; Bates, F. S.; Hamley, I. W.; Ryan, A. J.; Bras, W. Complex phase behavior of polyisoprene-polystyrene diblock copolymers near the orderdisorder transition. *Macromolecules* **1994**, *27*, 6922–6935.
- (42) Hajduk, D. A.; Takenouchi, H.; Hillmyer, M. A.; Bates, F. S.; Vigild, M. E.; Almdal, K. Stability of the perforated layer (PL) phase in diblock copolymer melts. *Macromolecules* **1997**, *30*, 3788–3795.
- (43) Squires, A. M.; Templer, R. H.; Seddon, J. M.; Woenckhaus, J.; Winter, R.; Finet, S.; Theyencheri, N. Kinetics and mechanism of the lamellar to gyroid inverse bicontinuous cubic phase transition. *Langmuir* **2002**, *18*, 7384–7392.
- (44) Rokhlenko, Y.; Gopinadhan, M.; Osuji, C. O.; Zhang, K.; O'Hern, C. S.; Larson, S. R.; Gopalan, P.; Majewski, P. W.; Yager, K. G. Magnetic alignment of block copolymer microdomains by intrinsic chain anisotropy. *Phys. Rev. Lett.* **2015**, *115*, 258302.
- (45) Keller, A.; Pedemonte, E.; Willmott, F. M. Macro-lattice from segregated amorphous phases of a three block copolymer. *Nature* **1970**, *225*, 538.
- (46) Manthis, A.; Hadzioannou, G.; Skoulios, A. Unit cell deformation under elongational stress of oriented sis three-block copolymers. *Polym. Eng. Sci.* **1977**, *17*, 570–572.
- (47) Kim, K.; Schulze, M. W.; Arora, A.; Lewis, R. M., III; Hillmyer, M. A.; Dorfman, K. D.; Bates, F. S. Thermal processing of diblock copolymer melts mimics metallurgy. *Science* **2017**, *356*, 520.
- (48) Cochran, E. W.; Bates, F. S. Shear-induced network-to-network transition in a block copolymer melt. *Phys. Rev. Lett.* **2004**, *93*, 087802.
- (49) Bates, F. S.; Hillmyer, M. A.; Lodge, T. P.; Bates, C. M.; Delaney, K. T.; Fredrickson, G. H. Multiblock polymers: panacea or pandora's box? *Science* **2012**, *336*, 434–440.
- (50) Jiang, Y.; Chen, J. Z. Y. Influence of chain rigidity on the phase behavior of wormlike diblock copolymers. *Phys. Rev. Lett.* **2013**, *110*, 138305.
- (51) Sun, T.; Liu, F.; Tang, P.; Qiu, F.; Yang, Y. Construction of rod-forming single network mesophases in rod-coil diblock copolymers via inversely designed phase transition pathways. *Macromolecules* **2018**, *51*, 5773–5787.
- (52) Yu, J.; Liu, F.; Tang, P.; Qiu, F.; Zhang, H.; Yang, Y. Effect of geometrical asymmetry on the phase behavior of rod-coil diblock copolymers. *Polymer* **2016**, *8*, 184.
- (53) Pryamitsyn, V.; Ganesan, V. Self-assembly of rod-coil block copolymers. *J. Chem. Phys.* **2004**, *120*, 5824–5838.
- (54) Tzeremes, G.; Rasmussen, K. Ø.; Lookman, T.; Saxena, A. Efficient computation of the structural phase behavior of block copolymers. *Phys. Rev. E* **2002**, *65*, 041806.
- (55) Tang, P.; Qiu, F.; Zhang, H.; Yang, Y. Phase separation patterns for diblock copolymers on spherical surfaces: a finite volume method. *Phys. Rev. E* **2005**, *72*, 016710.
- (56) Man, X.; Andelman, D.; Orland, H. Block copolymer at nanopatterned surfaces. *Macromolecules* **2010**, *43*, 7261–7268.

- (57) Hur, S.-M.; García-Cervera, C. J.; Kramer, E. J.; Fredrickson, G. H. SCFT simulations of thin film blends of block copolymer and homopolymer laterally confined in a square well. *Macromolecules* **2009**, *42*, 5861–5872.
- (58) Ceniceros, H. D.; Fredrickson, G. H. Numerical solution of polymer self-consistent field theory. *Multiscale Model. Simul.* **2004**, *2*, 452–474.
- (59) Kriksin, Y. A.; Khalatur, P. G. Parallel algorithm for 3D SCF simulation of copolymers with flexible and rigid blocks. *Macromol. Theory Simul.* **2012**, *21*, 382–399.
- (60) Weinan, E.; Ren, W.; Vanden-Eijnden, E. String method for the study of rare events. *Phys. Rev. B* **2002**, *66*, 052301.
- (61) Ren, W. Higher order string method for finding minimum energy paths. *Commun. Math. Sci.* **2003**, *1*, 377–384.
- (62) E, W.; Ren, W.; Vanden-Eijnden, E. Energy landscape and thermally activated switching of submicron-sized ferromagnetic elements. *J. Appl. Phys.* **2003**, *93*, 2275–2282.
- (63) Lin, L.; Cheng, X.; E, W.; Shi, A.-C.; Zhang, P. A numerical method for the study of nucleation of ordered phases. *J. Comput. Phys.* **2010**, *229*, 1797–1809.
- (64) Ji, N.; Tang, P.; Qiu, F.; Shi, A.-C. Kinetic pathways of lamellae to gyroid transition in weakly segregated diblock copolymers. *Macromolecules* **2015**, *48*, 8681–8693.
- (65) Cheng, X.; Lin, L.; E, W.; Zhang, P.; Shi, A.-C. Nucleation of ordered phases in block copolymers. *Phys. Rev. Lett.* **2010**, *104*, 148301.
- (66) E, W.; Ren, W.; Vanden-Eijnden, E. Simplified and improved string method for computing the minimum energy paths in barrier-crossing events. *J. Chem. Phys.* **2007**, *126*, 164103.
- (67) Arora, A.; Qin, J.; Morse, D. C.; Delaney, K. T.; Fredrickson, G. H.; Bates, F. S.; Dorfman, K. D. Broadly accessible self-consistent field theory for block polymer materials discovery. *Macromolecules* **2016**, *49*, 4675–4690.
- (68) Tang, J.; Jiang, Y.; Zhang, X.; Yan, D.; Chen, J. Z. Y. Phase diagram of rod-coil diblock copolymer melts. *Macromolecules* **2015**, *48*, 9060–9070.
- (69) Cai, Y.; Zhang, P.; Shi, A.-C. Liquid crystalline bilayers self-assembled from rod-coil diblock copolymers. *Soft Matter* **2017**, *13*, 4607–4615.
- (70) Li, S.; Jiang, Y.; Chen, J. Z. Y. Complex liquid-crystal nanostructures in semiflexible ABC linear triblock copolymers: a self-consistent field theory. *J. Chem. Phys.* **2016**, *145*, 184902.
- (71) Hannon, A. F.; Kline, R. J.; DeLongchamp, D. Advancing the computational methodology of rigid rod and semiflexible polymer systems: a new solution to the wormlike chain model with rod-coil copolymer calculations. *J. Polym. Sci., Part B: Polym. Phys.* **2019**, *57*, 29–39.
- (72) Zhao, W.; Russell, T. P.; Grason, G. M. Orientational interactions in block copolymer melts: self-consistent field theory. *J. Chem. Phys.* **2012**, *137*, 104911.
- (73) Matsen, M. W. Cylinder ↔ gyroid epitaxial transitions in complex polymeric liquids. *Phys. Rev. Lett.* **1998**, *80*, 4470–4473.
- (74) Matsen, M. W. Cylinder ↔ sphere epitaxial transitions in block copolymer melts. *J. Chem. Phys.* **2001**, *114*, 8165–8173.
- (75) Wang, C.; Jiang, K.; Zhang, P.; Shi, A.-C. Origin of epitaxies between ordered phases of block copolymers. *Soft Matter* **2011**, *7*, 10552.
- (76) Sun, T.; Tang, P.; Qiu, F.; Shi, A.-C. Emergence of ordered network mesophases in kinetic pathways of order-order transition for linear ABC triblock terpolymers. *Soft Matter* **2016**, *12*, 9769–9785.
- (77) Jiang, K.; Wang, C.; Huang, Y.; Zhang, P. Discovery of new metastable patterns in diblock copolymers. *Commun. Comput. Phys.* **2013**, *14*, 443–460.
- (78) Majewski, P. W.; Yager, K. G. Reordering transitions during annealing of block copolymer cylinder phases. *Soft Matter* **2016**, *12*, 281–294.
- (79) Yager, K. G.; Forrey, C.; Singh, G.; Satija, S. K.; Page, K. A.; Patton, D. L.; Douglas, J. F.; Jones, R. L.; Karim, A. Thermally-induced transition of lamellae orientation in blockcopolymer films on ‘neutral’ nanoparticle-coated substrates. *Soft Matter* **2015**, *11*, 5154–5167.
- (80) Ashcroft, N. W.; Mermin, N. D. *Solid state physics*; New York: Holt, 1976, pp 91–93.
- (81) Yadav, M.; Bates, F. S.; Morse, D. C. Network model of the disordered phase in symmetric diblock copolymer melts. *Phys. Rev. Lett.* **2018**, *121*, 127802.
- (82) Vidil, T.; Hampu, N.; Hillmyer, M. A. Nanoporous thermosets with percolating pores from block polymers chemically fixed above the order-disorder transition. *ACS Cent. Sci.* **2017**, *3*, 1114–1120.
- (83) Majewski, P. W.; Yager, K. G. Rapid ordering of block copolymer thin films. *J. Phys.: Condens. Matter* **2016**, *28*, 403002.